Ab Initio Scattering Calculation in Three-Body Coulomb Systems: e^+−H, e^-−$\bar{\text{H}}$ and e^+−He^+

V. A. Gradusov, V. A. Roudnev, E. A. Yarevsky and S. L. Yakovlev

Department of Computational Physics, St. Petersburg State University, 7/9 Universitetskaya nab., St. Petersburg, 199034, Russia

Abstract

We present the results of our detailed calculations of scattering characteristics in $e^-e^+\bar{p}$ (e^-e^+p) and $e^+e^-\text{He}^{++}$ systems with zero total orbital momentum by direct solving the Faddeev–Merkuriev equations in the differential form. We calculate all possible cross-sections in the low-energy region which admits up to seven open channels including the rearrangement channels of ground and excited states of antihydrogen, positronium and helium ion formations. All sharp resonances of the systems obtained and approved previously by a number of authors are clearly reproduced in the calculated cross sections. Alternatively, the exterior complex scaling approach has been used for calculating resonant energies. It confirmed the existence of reported by other authors broad resonances in the $e^+e^-\text{He}^{++}$ system. Prominent oscillations of Gailitis–Damburg type have been found in cross sections for energies above the threshold corresponding to $n = 2$ state of antihydrogen.

Keywords: *Faddeev–Merkuriev equations; positron scattering; antihydrogen formation; Gailitis–Damburg oscillations*

1 Introduction

Study of electron and positron scattering off light atomic targets (like (anti)hydrogen atom and helium cation) is of fundamental importance for atomic physics. These colliding systems represent genuine three-body Coulombic systems with variety of channels, rich resonant structure of scattering cross sections and the fundamental rearrangement phenomenon of positronium (electron-positron bound state) formation. For such a case the solution methods should be capable of representing the solution for all the asymptotic fragmentations accurately. The Faddeev equations [1] and their generalization to the long-range Coulomb case, the so-called Faddeev–Merkuriev (FM) equations [2], were designed especially to fulfill this requirement. This generalization is based on the Coulomb potential splitting into the interior and the long range tail parts leading to the mathematically rigorous boundary value problem, which solution

Proceedings of the International Conference 'Nuclear Theory in the Supercomputing Era — 2018' (NTSE-2018), Daejeon, South Korea, October 29 – November 2, 2018, eds. A. M. Shirokov and A. I. Mazur. Pacific National University, Khabarovsk, Russia, 2019, p. 137.

http://www.ntse.khb.ru/files/uploads/2018/proceedings/Yakovlev.pdf.

is strictly equivalent to the solution of the Schrödinger equation [1]. This approach suits the computationally difficult detailed low-energy elastic and reactive scattering calculations in three-body Coulomb systems perfectly [3–5].

Here, the formalism of FM equations is used to calculate the S-wave cross sections in $e^-e^+\bar{p}$ (e^-e^+p) and $e^+e^-\mathrm{He}^{++}$ systems in the low-energy region for all open channels. Even though there are many calculations available in the literature [3, 4, 6–17], there is still some lack of high-precision and detailed results especially for the $e^+e^-\mathrm{He}^{++}$ system, which is one of the motivations for performing this research. Besides, a special emphasis is made on the antihydrogen formation by antiproton impact of positronium which is currently used in experiments on antimatter at CERN (see Ref. [18] and references therein).

The paper is organized as follows. In Section 2, we give the necessary portion of the three-body FM equations formalism and briefly describe the respective solution technique in the case of zero total orbital momentum of the system. Section 3 contains results of calculations of low-energy reactive scattering in $e^-e^+\bar{p}$ (e^-e^+p) and $e^+e^-\mathrm{He}^{++}$ systems. The last Section concludes the paper.

We use atomic units throughout the paper. The magnitude of a vector $\boldsymbol{x}$ is denoted by x, i. e., $x = |\boldsymbol{x}|$, and $\hat{\boldsymbol{x}} = \boldsymbol{x}/x$ stands for the unit vector. The set of indices $\{\alpha, \beta, \gamma\}$ runs over the set $\{1, 2, 3\}$ enumerating particles and is also used for identifying the complementary pair of particles since the pair of particles $\beta\gamma$ in the partition $\{\alpha(\beta\gamma)\}$ is uniquely determined by the particle α.

2 Theory and numerical solution

We consider a system of three spinless nonrelativistic charged particles of masses m_α and charges Z_α, $\alpha = 1, 2, 3$. Standard Jacobi coordinates are defined for a partition $\alpha(\beta\gamma)$ as the relative position vectors between the particles of the pair $\beta\gamma$ and between their center of mass and the particle α. In applications, it is convenient to use the reduced Jacobi coordinates $\boldsymbol{x}_\alpha, \boldsymbol{y}_\alpha$ which are Jacobi vectors scaled by the factors $\sqrt{2\mu_\alpha}$ and $\sqrt{2\mu_{\alpha(\beta\gamma)}}$, respectively, where the reduced masses are given by

$$\mu_\alpha = \frac{m_\beta\, m_\gamma}{m_\beta + m_\gamma}, \qquad \mu_{\alpha(\beta\gamma)} = \frac{m_\alpha(m_\beta + m_\gamma)}{m_\alpha + m_\beta + m_\gamma}. \tag{1}$$

The reduced Jacobi vectors for different choices of α are related by an orthogonal transformation,

$$\boldsymbol{x}_\beta = c_{\beta\alpha}\, \boldsymbol{x}_\alpha + s_{\beta\alpha}\, \boldsymbol{y}_\alpha, \qquad \boldsymbol{y}_\beta = -s_{\beta\alpha}\, \boldsymbol{x}_\alpha + c_{\beta\alpha}\, \boldsymbol{y}_\alpha, \tag{2}$$

where

$$c_{\beta\alpha} = -\left[\frac{m_\beta\, m_\alpha}{(M - m_\beta)(M - m_\alpha)}\right]^{1/2}, \qquad s_{\beta\alpha} = (-1)^{\beta-\alpha}\mathrm{sgn}(\alpha - \beta)(1 - c_{\beta\alpha}^2)^{1/2},$$

and $M = \sum_\alpha m_\alpha$. In what follows, it is assumed that the β Jacobi vectors are represented through the α vectors via Eq. (2).

In the reduced Jacobi coordinates, the FM equations for three charged particles [1]

read

$$\big\{T_\alpha + V_\alpha(x_\alpha) + \sum_{\beta\neq\alpha} V_\beta^{(\mathrm{l})}(x_\beta, y_\beta) - E\big\}\psi_\alpha(\boldsymbol{x_\alpha}, \boldsymbol{y_\alpha}) = -V_\alpha^{(\mathrm{s})}(x_\alpha, y_\alpha) \sum_{\beta\neq\alpha} \psi_\beta(\boldsymbol{x_\beta}, \boldsymbol{y_\beta}). \tag{3}$$

Here $T_\alpha \equiv -\Delta_{\boldsymbol{x_\alpha}} - \Delta_{\boldsymbol{y_\alpha}}$ are the kinetic energy operators. In this paper, the potentials V_α represent the pairwise Coulomb interaction $V_\alpha(x_\alpha) = \sqrt{2\mu_\alpha} Z_\beta Z_\gamma / x_\alpha$ $(\beta, \gamma \neq \alpha)$, although, generally, a short-range (decreasing as $1/x_\alpha^2$ or faster as $x_\alpha \to \infty$) potential can also be included in the formalism. The potentials V_α are split into the interior (short-range) $V_\alpha^{(\mathrm{s})}$ and the tail (long-range) parts $V_\alpha^{(\mathrm{l})}$,

$$V_\alpha(x_\alpha) = V_\alpha^{(\mathrm{s})}(x_\alpha, y_\alpha) + V_\alpha^{(\mathrm{l})}(x_\alpha, y_\alpha). \tag{4}$$

Equations (3) can be summed up leading to the Schrödinger equation for the wave function $\Psi = \sum_\alpha \psi_\alpha$, where ψ_α are the components of the wave function given by the solution of Eqs. (3).

Splitting Eq. (4) for the potentials in general case is done in the three-body configuration space by the Merkuriev cut-off function χ_α [1],

$$V_\alpha^{(\mathrm{s})}(x_\alpha, y_\alpha) = \chi_\alpha(x_\alpha, y_\alpha)\, V_\alpha(x_\alpha). \tag{5}$$

This splitting confines the short-range part of the potential to the regions in the three-body configuration space corresponding to the three-body collision point (particles are close to each other) and the binary configuration ($x_\alpha \ll y_\alpha$ when $y_\alpha \to \infty$). The form of the cut-off function can be rather arbitrary within some general requirements [2,5]. In the paper [19], we have shown, that for the energies below the breakup threshold, it is practical to confine the cut-off function to the two-body configuration space. Thus in this paper, for actual calculations we use the cut-off function of the form

$$\chi_\alpha(x_\alpha) = 2/\big\{1 + \exp\big[(x_\alpha/x_{0\alpha})^{2.01}\big]\big\}, \tag{6}$$

where $x_{0\alpha}$ is a parameter. With this smoothed Heaviside step function, the split potentials $V_\alpha^{(\mathrm{s,l})}$ become two-body quantities $V_\alpha^{(\mathrm{s,l})} = V_\alpha^{(\mathrm{s,l})}(x_\alpha)$.

The splitting procedure makes the properties of the FM equations for Coulomb potentials as appropriate for scattering problems as the standard Faddeev equations in the case of short-range potentials [4]. With the described above choice of the short-range part of the potential $V^{(\mathrm{s})}$, the right-hand side of each Eq. (3) is confined to the vicinity of the three-body collision point [20], which is the key property of the FM equations. It leads to the asymptotic uncoupling of the set of FM equations and, accordingly, the asymptotics of each component ψ_α for energies below the breakup threshold contains only the terms corresponding to the binary configurations of pairing α [4, 20].

The total orbital momentum is an integral of motion for the three-particle system. This makes it possible to reduce the set of FM equations by projecting Eq. (3) onto a subspace of a given total angular momentum [14]. In this article we consider the case of zero total orbital momentum of the system. The kinetic energy operator in the left-hand side of Eq. (3) on the subspace of zero total orbital momentum has the form

$$T_\alpha = -\frac{\partial^2}{\partial y_\alpha^2} - \frac{2}{y_\alpha}\frac{\partial}{\partial y_\alpha} - \frac{\partial^2}{\partial x_\alpha^2} - \frac{2}{x_\alpha}\frac{\partial}{\partial x_\alpha} - \left(\frac{1}{y_\alpha^2} + \frac{1}{x_\alpha^2}\right)\frac{\partial}{\partial z_\alpha}(1 - z_\alpha^2)\frac{\partial}{\partial z_\alpha}, \tag{7}$$

where $z_\alpha \equiv \cos(\hat{\boldsymbol{x}}_\alpha \cdot \hat{\boldsymbol{y}}_\alpha)$. The corresponding projection of the component ψ_α depends only on the coordinates $X_\alpha = \{x_\alpha, y_\alpha, z_\alpha\}$ in the plane containing all three particles. By choosing the coordinate system appropriately, its asymptotics for energies E below the three-body ionization threshold can be written as

$$\psi_\alpha(X_\alpha) \sim -\frac{\phi_{n_0\ell_0}(x_\alpha)}{x_\alpha\, y_\alpha}\, Y_{\ell_0 0}(\theta_\alpha, 0)\, \mathrm{e}^{-\mathrm{i}\vartheta_{\ell_0}(y_\alpha, p_{n_0})}\, \delta_{\alpha,\alpha_0} + \sum_{n\ell} \frac{\phi_{n\ell}(x_\alpha)}{x_\alpha\, y_\alpha}\, Y_{\ell 0}(\theta_\alpha, 0) \sqrt{\frac{p_{n_0}}{p_n}}\, S_{n\ell,n_0\ell_0}\, \mathrm{e}^{+\mathrm{i}\vartheta_\ell(y_\alpha, p_n)}, \quad (8)$$

where the set of indices $\{n\ell\}$ specifies various two-body Coulomb bound states in the pair α (that is, binary scattering channels $\{\alpha; n\ell\}$) with the wave function $\phi_{n\ell}(x_\alpha)\, Y_{\ell m}(\hat{\boldsymbol{x}})/x_\alpha$ and the energy ε_n. Here $Y_{\ell m}(\hat{\boldsymbol{x}})$ stands for the standard spherical harmonic function. The momentum p_n of the outgoing particle is determined by the energy conservation condition $E = p_n^2 + \varepsilon_n$. The Coulomb distorted wave phase $\vartheta_\ell(y_\alpha, p_n) \equiv p_n y_\alpha - \eta_n \log(2p_n y_\alpha) - \ell\pi/2 + \sigma_n$, where $\sigma_n = \arg\Gamma(1 + \mathrm{i}\eta_n)$ and the Sommerfeld parameter is defined as $\eta_n \equiv Z_\alpha(Z_\beta + Z_\gamma)\sqrt{2m_{\alpha(\beta\gamma)}}/(2p_n)$. Finally, $S_{n\ell,n_0\ell_0}$ are the S-matrix elements.

To reduce the computational cost of solving the system of FM equations (3), several modifications has been done. First, since the potential V_3 is repulsive and the corresponding two-body Hamiltonian does not support any bound state, this potential is included in the left-hand side of Eqs. (3), thus reducing the number of these equations from 3 to 2. Formally, it is done by setting $\chi_3 = 0$. Secondly, the asymptotic particle-atom Coulomb potential $V_\alpha^{\mathrm{eff}}(y_\alpha) = 2p_n\eta_n/y_\alpha$ is introduced explicitly in Eqs. (3) for treating the asymptotic Coulomb singularity,

$$\big\{T_\alpha + V_\alpha(x_\alpha) + V_\alpha^{\mathrm{eff}}(y_\alpha) - E\big\}\psi_\alpha(X_\alpha) = -V_\alpha^{(\mathrm{s})}(x_\alpha)\, \psi_\beta(X_\beta) - \big[V_\beta^{(1)}(x_\beta) + V_3(x_3) - V_\alpha^{\mathrm{eff}}(y_\alpha)\big]\psi_\alpha(X_\alpha), \quad (9)$$

where $\beta \neq \alpha = 1, 2$. After that the Coulomb singularity can be effectively inverted [21]. Another modification is done to make the solutions of Eqs. (3) to be real functions. This is achieved by using the asymptotic conditions with standing waves instead of conditions (8).

The FM equations are solved by the spline collocation method [22] in a box $[0, R_\alpha^x] \times [0, R_\alpha^y] \times [-1, 1]$ for each component ψ_α. As a basis set for expanding the components, we use products of basis functions in the space of quintic Hermite splines S_5^3 (splines of degree 5 with 2 continuous derivatives) in each coordinate. Each basis function is local and nonzero only on two adjoining intervals of the grid. As a result, the matrix of the system of linear equations for expansion coefficients is sparse. It is solved by the Arnoldi iterations in GMRES variant [23] with right preconditioning by the discretized version of the operators in the left-hand side of the system of FM equations. To invert the preconditioner, we use the algorithm which is known as the "tensor trick" or matrix decomposition method [22, 24, 25]. It provides a fast diagonalization of the matrix using its tensor product structure. For a more detailed description of our computational method, we refer the reader to Ref. [21].

3 Results

3.1 Scattering in $e^-e^+\bar{p}$ and e^+e^-p systems

The positron-hydrogen atom scattering is the simplest example of positron-atom scattering process. Many calculations are available in the literature [3, 7, 9–13, 15, 16, 18]. The renewed interest in studying reactions involving the positron, electron and (anti)proton is motivated by experiments on antimatter ongoing at CERN [18]. The reaction of the antihydrogen production via the antiproton ($\bar{p}$) impact on positronium atom (Ps, the bound state of e^+ and e^-) plays the key role in antimatter formation. Due to the symmetry of particle charges, the cross sections in e^+e^-p and $e^-e^+\bar{p}$ systems are identical. Below in this section we refer to the $e^+e^-\bar{p}$ system.

By solving the FM equations, we have calculated the cross sections for all possible scattering processes in the $e^+e^-\bar{p}$ system in the total energy range between the energies of the atomic states $\bar{\mathrm{H}}(n=1)$ and $\bar{\mathrm{H}}(n=3)$, i. e., from -0.49973 a.u. to -0.05553 a.u. with the step in energy of 0.0007 a.u. Within this energy interval, the elastic scattering, excitation and rearrangement processes leading to the $\bar{\mathrm{H}}(n=1,2)$ and $\mathrm{Ps}(n=1,2)$ atomic states are possible. The energies of these atomic states form the thresholds for scattering channels. The maximal number of open channels in the energy interval between the $\mathrm{Ps}(n=2)$ and $\bar{\mathrm{H}}(n=3)$ states equals to 6. The accuracy of our calculations guarantees that the uncertainties of the obtained cross sections are less than 1%. A calculation of all cross sections for each energy value from this interval requires a time of approximately 3 hours on a SMP node with 32 cores and 20 Gb RAM. We have a system of 3,241,020 linear equations and the respective matrix has 432 nonzero elements in a row.

We compare our results in Table 1 with tabulated results of other authors and present some additional cross sections for further references. In this Table and in the text below we use shortcuts $\bar{\mathrm{H}}(n)$ and $\bar{\mathrm{H}}(n,\ell)$ for the atomic states with the principal quantum number n and the orbital momentum ℓ. Some of all possible 36 cross sections for the collision processes with $e^-{-}\bar{\mathrm{H}}$ and $\bar{p}{-}\mathrm{Ps}$ configurations in the entrance and final channels are presented in Fig. 1.

The antihydrogen production cross sections in the energy region between the $\bar{\mathrm{H}}(2)$ and $\bar{\mathrm{H}}(3)$ thresholds are studied in detail in a recent work [18]. These cross sections are compared with our results in Fig. 2. The resonances manifest themselves in Figs. 1 and 2 as peaks in some of the calculated cross sections. The resonance energies found by different methods [26–29] are known with a good accuracy. We mark their positions in the figures by vertical dashed lines. All resonances are clearly seen in the calculated cross sections. The $\bar{p}+\mathrm{Ps}(1,s)\to\bar{p}+\mathrm{Ps}(1,s)$ and $e^-+\bar{\mathrm{H}}(2,s)\to e^-+\bar{\mathrm{H}}(2,p)$ cross sections as well as the $e^-+\bar{\mathrm{H}}(2,s)\to e^-+\bar{\mathrm{H}}(2,s)$ cross section not shown in the figure, have sharp minima which also look like resonances but do not coincide with any of the known resonance positions. We agree with the interpretation of these minima suggested in Ref. [10] where they were associated with the Ramsauer–Townsend effect.

A special attention should be paid to the oscillations of the cross sections just above the $\bar{\mathrm{H}}(2)$ threshold in Fig. 2. We give more detailed plots of the $\bar{p}+\mathrm{Ps}(1)\to e^-+\bar{\mathrm{H}}(1)$ and $\bar{p}+\mathrm{Ps}(1)\to e^-+\bar{\mathrm{H}}(2)$ cross sections in the energy region above this threshold in Fig. 3. Prominent oscillations of both cross sections and their character suggest to associate these oscillations with the phenomenon predicted in Refs. [30,31]. According to Refs. [30,31], the energy position E_n of the nth maximum of the oscillations follows

Table 1: Our results for scattering cross sections in the $e^-e^+\bar{p}$ system in comparison with that of other authors (energies are given relative to the $\bar{\mathrm{H}}(1)$ threshold at -0.49973 a.u.).

E, a.u.	0.27026	0.28140	0.32017	0.36145	0.385	0.40	0.415	0.42
$\sigma_{e^-+\bar{\mathrm{H}}(1)\to e^-+\bar{\mathrm{H}}(1)}$	0.0353	0.0417	0.0634	0.0836	0.0944	0.100	0.105	0.107
[10]			0.0651	0.0844		0.100		
[3]	0.0372	0.0429	0.0649	0.0866	0.090	0.096	0.099	0.101
[9]		0.0431	0.0650	0.0856				
$\sigma_{e^-+\bar{\mathrm{H}}(1)\to\bar{p}+\mathrm{Ps}(1)}$	0.00412	0.00430	0.00487	0.00562	0.00565	0.00572	0.00575	0.00574
[10]			0.00490	0.00567		0.00581		
[3]	0.00410	0.00439	0.00487	0.00557				
[9]		0.00422	0.00481	0.00554				
$\sigma_{\bar{p}+\mathrm{Ps}(1)\to\bar{p}+\mathrm{Ps}(1)}$	3.49	7.06	9.87	8.31	7.11	6.44	5.82	5.62
[10]			9.87	8.32		6.45		
[3]	3.500	7.060	9.866	8.312	7.09	6.44	5.83	5.63
[9]		6.936	9.868	8.332				
$\sigma_{\bar{p}+\mathrm{Ps}(1)\to e^-+\bar{\mathrm{H}}(1)}$	0.0272	0.0191	0.0111	0.0091	0.00806	0.00763	0.00724	0.00709
[3]	0.0274	0.0195	0.0111	0.0091	0.00815	0.00780	0.00729	0.00715
$\sigma_{e^-+\bar{\mathrm{H}}(1)\to e^-+\bar{\mathrm{H}}(2,s)}$					0.000662	0.00137	0.00206	0.00228
$\sigma_{e^-+\bar{\mathrm{H}}(1)\to e^-+\bar{\mathrm{H}}(2,p)}$					0.000399	0.000236	0.000421	0.000582
$\sigma_{e^-+\bar{\mathrm{H}}(2,s)\to\bar{p}+\mathrm{Ps}(1,s)}$					1.26	0.576	0.477	0.475
$\sigma_{e^-+\bar{\mathrm{H}}(2,s)\to e^-+\bar{\mathrm{H}}(1,s)}$					0.0249	0.0217	0.0212	0.0212
$\sigma_{\bar{p}+\mathrm{Ps}(1)\to e^-+\bar{\mathrm{H}}(2,s)}$					0.0476	0.0484	0.0581	0.0631
$\sigma_{\bar{p}+\mathrm{Ps}(1)\to e^-+\bar{\mathrm{H}}(2,p)}$					0.0390	0.0484	0.0512	0.0519

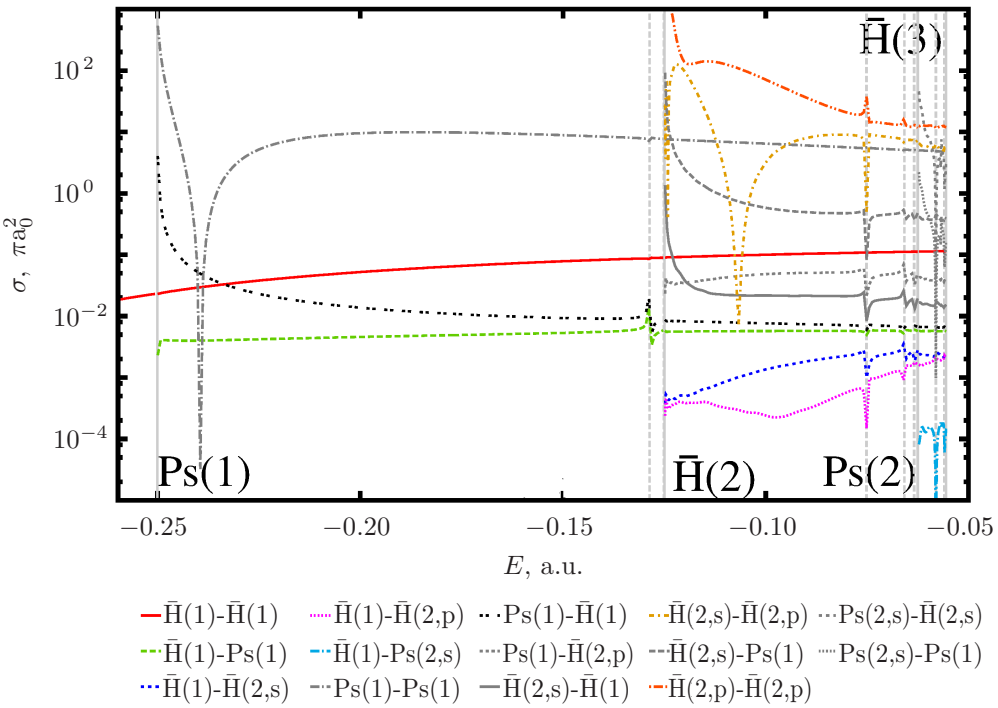

Figure 1: Cross sections in the $e^-e^+\bar{p}$ system. Vertical solid lines show the binary thresholds, vertical dashed lines mark resonances positions. We use the notation $\mathrm{Ps}(n_1,\ell_1)$–$\bar{\mathrm{H}}(n_2,\ell_2)$ to specify the reaction $\bar{p}+\mathrm{Ps}(n_1,\ell_1)\to e^-+\bar{\mathrm{H}}(n_2,\ell_2)$ and similar notations for other reactions.

the rule

$$\log(E_n - E_{\mathrm{th}}) = An + B, \tag{10}$$

where A and B are constants and E_{th} is the threshold energy. We plot the respective quantities for the $\bar{p}+\mathrm{Ps}(1)\to e^-+\bar{\mathrm{H}}(1)$ and $\bar{p}+\mathrm{Ps}(1)\to e^-+\bar{\mathrm{H}}(2)$ cross section oscillations near the threshold in panels (c)–(e) in Fig. 3. Clearly, the linear spacing of $\log(E_n-E_{\mathrm{th}})$ is nearly perfect in both cases of rearrangement cross sections except for the last points. The latter probably indicate the range of validity of approximations made in Ref. [30,31] leading to Eq. (10). As for the $\bar{p}+\mathrm{Ps}(2)\to e^-+\bar{\mathrm{H}}(n\le 2)$ cross section behavior shown in the right panel of Fig. 2, we obviously cannot make such a quantitative analysis as of the above threshold oscillations. Nevertheless, we can agree with Ref. [18] that there is an oscillation at the energy close to -0.06194 a.u., which was also found earlier in Ref. [32]. It should be noted that the elastic cross section oscillations for the $\mathrm{Ps}-p$ scattering above the Ps(2) threshold were also found recently in Ref. [33].

3.2 Scattering in $e^+e^-\mathrm{He}^{++}$ system

The scattering of positron by positive helium ion is an example of the positron–atomic target scattering in which the asymptotic Coulomb interaction is present in one of

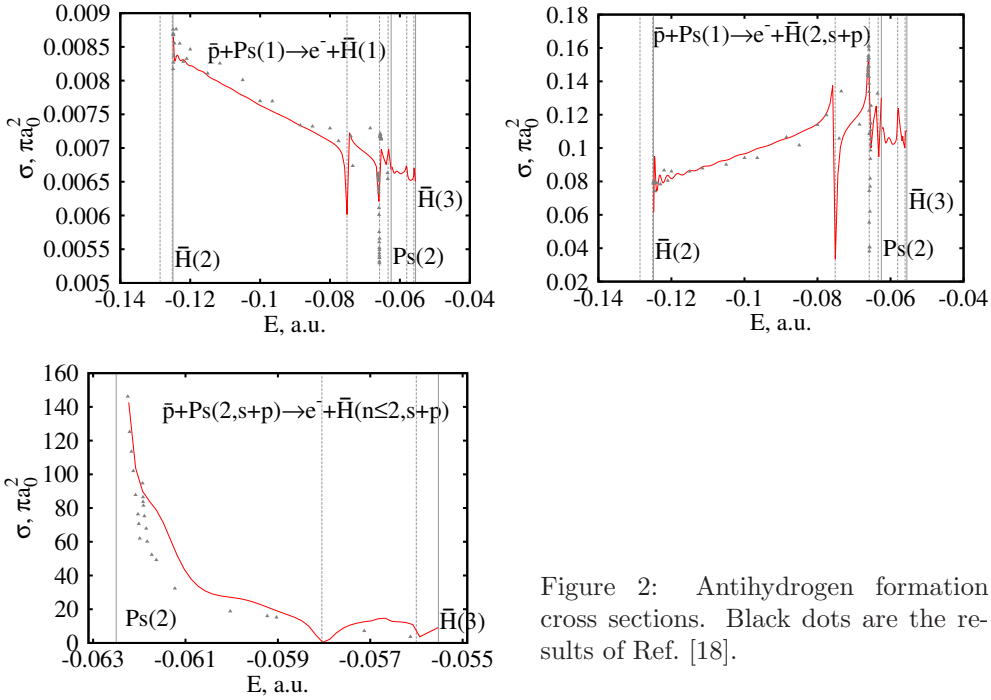

Figure 2: Antihydrogen formation cross sections. Black dots are the results of Ref. [18].

the configurations. There is a number of respective calculations in a wide energy region [34–36]. However, to the best of our knowledge, there is lack of published results of calculations in the low-energy region. In this work, by solving the FM equations, we have calculated cross sections for all possible scattering processes in the $e^+e^-\mathrm{He}^{++}$ system in the entire energy range between the energy thresholds of the $\mathrm{He}^+(1)$ and $\mathrm{He}^+(4)$ states, i. e., from -1.9997 a.u. to -0.12496 a.u. with the step in energy of 0.0007 a.u. In this energy interval, the elastic, excitation and rearrangement processes leading to the $\mathrm{He}^+(n=1,2,3)$ and $\mathrm{Ps}(n=1)$ atomic states are possible. As in the previous case, the accuracy of our calculations guarantees that the uncertainties of the obtained cross sections are not exceeding 1%.

The calculated 11 of all 49 cross sections are given in Table 2. The energy dependences of the cross sections for the reactions $e^+ - \mathrm{He}^+ \to e^+ - \mathrm{He}^+$, $e^+ - \mathrm{He}^+ \to \mathrm{He}^{++} - \mathrm{Ps}$ and $\mathrm{He}^{++} - \mathrm{Ps} \to \mathrm{He}^{++} - \mathrm{Ps}$, $\mathrm{He}^{++} - \mathrm{Ps} \to e^+ - \mathrm{He}^+$ are displayed in Fig. 4.

Resonance energies in the $e^+e^-\mathrm{He}^{++}$ system are far lesser-known, there is a number of disagreements between the published results, see, e. g., Refs. [37–39] and references therein. Most of the authors agree that there are two broad resonances at the energies of -0.371 a.u. and -0.188 a.u. [38] and one narrow resonance slightly below the positronium ground state formation threshold at -0.250 a.u. [38,39]. The positions of these resonances are marked in Fig. 4 by dashed vertical lines (the dashed vertical line at -0.250 a.u. almost coincides with the vertical line showing the positronium ground state threshold and is not visible). We do not see a usual singular behavior of the cross sections in the vicinity of the narrow resonance. However, at the same time, one can see that the $e^+ + \mathrm{He}^+(1) \to \mathrm{He}^{++} + \mathrm{Ps}(1)$ cross section does not follow the well-known law of threshold behavior at the Ps(1) threshold at -0.25 a.u. The

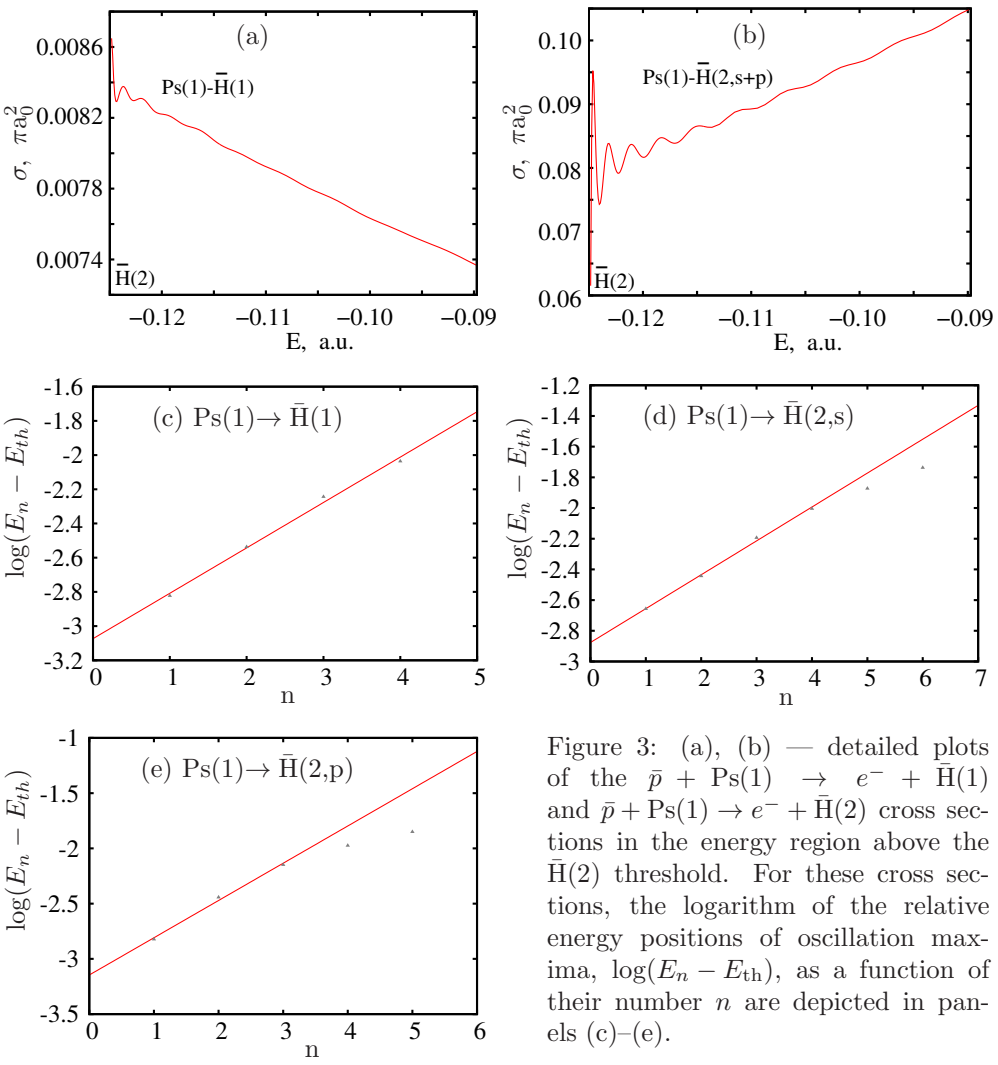

Figure 3: (a), (b) — detailed plots of the $\bar{p}$ + Ps(1) → e^- + $\bar{\mathrm{H}}(1)$ and $\bar{p} + \mathrm{Ps}(1) \to e^- + \bar{\mathrm{H}}(2)$ cross sections in the energy region above the $\bar{\mathrm{H}}(2)$ threshold. For these cross sections, the logarithm of the relative energy positions of oscillation maxima, $\log(E_n - E_{\mathrm{th}})$, as a function of their number n are depicted in panels (c)–(e).

cross section should tend to zero linearly as $p \to 0$ where p is the relative momentum between the target and the projectile [40], but it grows up to some constant value instead. This anomalous behavior can be a sign of a resonance. The broad resonances are not manifested in the cross sections as expected.

To check the existence of the broad resonances, we have used another approach based on the complex rotation method [41] applied to the Schrödinger equation. We have found these broad resonances; their positions and widths are given in Table 3 and compared with the results of Ref. [38].

The sharp local minimum is seen again in the $\mathrm{He}^{++} + \mathrm{Ps}(1) \to \mathrm{He}^{++} + \mathrm{Ps}(1)$ cross section for the direct process with neutral target. As in the previous Subsection, we associate this minimum with the Ramsauer–Townsend effect.

Table 2: Scattering cross sections in the $e^+e^-\mathrm{He}^{++}$ system (energies are given relative to the $\mathrm{He}^+(1)$ threshold at -1.9997 a.u.). We use a notation $a(b)$ for $a \cdot 10^b$.

E, a.u.	1.55	1.60	1.65	1.70	1.77	1.80	1.83	1.86
$\sigma_{e^+ + \mathrm{He}^+(1) \to e^+ + \mathrm{He}^+(1)}$	0.000855	0.00101	0.00116	0.00133	0.00158	0.00168	0.00178	0.00188
$\sigma_{e^+ + \mathrm{He}^+(1) \to e^+ + \mathrm{He}^+(2,s)}$	$\sim$1(-9)	$\sim$1(-8)	2(-7)	6(-7)	2.6(-6)	4.4(-6)	6.9(-6)	1.1(-5)
$\sigma_{e^+ + \mathrm{He}^+(1) \to e^+ + \mathrm{He}^+(2,p)}$	$\sim$ 1(-10)	$\sim$1-(8)	3(-7)	2.5(-6)	1.1(-5)	1.8(-5)	2.6(-5)	3.6(-5)
$\sigma_{e^+ + \mathrm{He}^+(1) \to \mathrm{He}^{++} + \mathrm{Ps}(1)}$					1(-7)	1(-7)	2(-7)	3(-7)
$\sigma_{\mathrm{He}^{++} + \mathrm{Ps}(1) \to \mathrm{He}^{++} + \mathrm{Ps}(1)}$					20.6	19.6	8.82	3.00
$\sigma_{\mathrm{He}^{++} + \mathrm{Ps}(1) \to e^+ + \mathrm{He}^+(2,s)}$					0.366	0.102	0.0433	0.0199
$\sigma_{\mathrm{He}^{++} + \mathrm{Ps}(1) \to e^+ + \mathrm{He}^+(2,p)}$					0.0944	0.0214	0.00876	0.00584
$\sigma_{e^+ + \mathrm{He}^+(2,s) \to e^+ + \mathrm{He}^+(2,s)}$	1.12	3.35	6.64	6.63	5.11	4.59	4.10	3.66
$\sigma_{e^+ + \mathrm{He}^+(2,p) \to e^+ + \mathrm{He}^+(2,s)}$	5.34	4.57	2.76	1.35	0.866	0.832	0.820	0.815
$\sigma_{e^+ + \mathrm{He}^+(3,s) \to e^+ + \mathrm{He}^+(3,s)}$						9.87	18.4	11.7
$\sigma_{e^+ + \mathrm{He}^+(3,s) \to e^+ + \mathrm{He}^+(3,p)}$						15.7	1.62	1.21

Table 3: Energies of broad resonances in the $e^+e^-\mathrm{He}^{++}$ system and their widths, (E_r, Γ) (in a.u.).

Present work	$(-0.3704, 0.1297)$	$(-0.1857, 0.0395)$
[38]	$(-0.3705, 0.1294)$	$(-0.1856, 0.0393)$

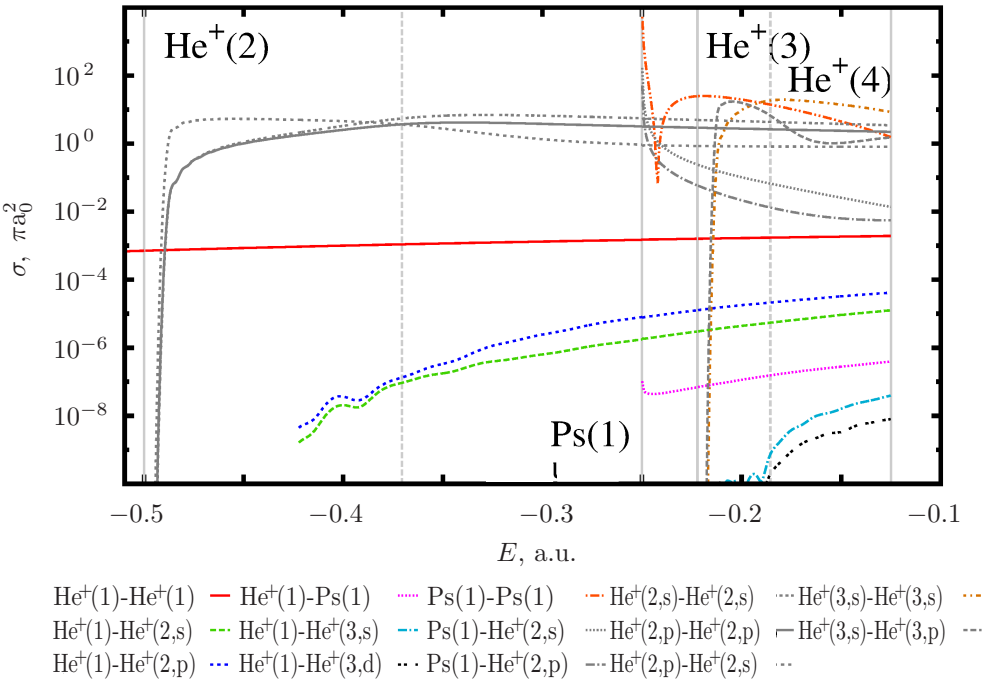

Figure 4: Cross sections in the $e^-e^+\mathrm{He}^+$ system. Vertical solid lines show the binary thresholds, vertical dashed lines mark resonance positions. We use the notation $\mathrm{Ps}(n_1,\ell_1)$–$\mathrm{He}^+(n_2,\ell_2)$ to specify the reaction $\mathrm{He}^{++}+\mathrm{Ps}(n_1,\ell_1)\to e^++\mathrm{He}^+(n_2,\ell_2)$ and similar notations for other reactions.

4 Conclusions

In this paper, detailed calculations of low-energy reactive scattering in the $e^-e^+\bar{p}$ and $e^+e^-\mathrm{He}^{++}$ systems in the case of zero total orbital momentum have been performed with the use of the FM equations in the total orbital momentum representation.

The calculated cross sections in the $e^-e^+\bar{p}$ system reproduce all known resonant peaks. The Gailitis–Damburg oscillations of the $\bar{p}+\mathrm{Ps}(1)\to e^-+\bar{\mathrm{H}}(1)$ and $\bar{p}+\mathrm{Ps}(1)\to e^-+\bar{\mathrm{H}}(2)$ cross sections just above the $\bar{\mathrm{H}}(2)$ threshold are discovered and the theory of the energy distribution of the oscillation maxima with respect to the threshold is verified.

The two known broad resonances [38] in the $e^+e^-\mathrm{He}^{++}$ system do not contribute to the cross section. We suggest to explain the anomalous threshold behavior of the $e^+ + \mathrm{He}^+(1) \to \mathrm{He}^{++} + \mathrm{Ps}(1)$ cross section by the existence of the narrow resonance found in Refs. [38, 39].

We have demonstrated that the formalism of FM equations is efficient for calculating elastic and reactive scattering in three-body atomic systems. The extension of the current approach to nonzero total orbital momentum case is now in progress.

Acknowledgments

This work is supported by the Russian Foundation for Basic Research grant No. 18-02-00492. The calculations were performed using the resources of the Computational Center of St. Petersburg State University.

References

[1] L. D. Faddeev and S. P. Merkuriev, *Quantum scattering theory for several particle systems*. Kluwer, Dordrech, 1993.

[2] S. P. Merkuriev, Ann. Phys. **130**, 395 (1980).

[3] C.-Y. Hu, J. Phys. B **32**, 3077 (1999).

[4] Z. Papp, C.-Y. Hu, Z. T. Hlousek, B. Konya and S. L. Yakovlev, Phys. Rev. A **63**, 062721 (2001).

[5] A. A. Kvitsinsky, J. Carbonell and C. Gignoux, Phys. Rev. A **46**, 1310 (1992).

[6] A. K. Bhatia, A. Temkin and H. Eiserike, Phys. Rev. A **9**, 219 (1974).

[7] J. W. Humberston, P. Van Reeth, M. S. T. Watts and W. E. Meyerhof, J. Phys. B **30**, 2477 (1997).

[8] M. Charlton and J. W. Humberston, *Positron physics*. Cambridge University Press, 2001.

[9] T. T. Gien, Phys. Rev. A **59**, 1238 (1999).

[10] J. Mitroy and K. Ratnavelu, J. Phys. B **28**, 287 (1995).

[11] A. S. Kadyrov and I. Bray, Phys. Rev. A **66**, 012710 (2002).

[12] A. Igarashi and N. Toshima, Phys. Rev. A **50**, 232 (1994).

[13] S. J. Ward and J. Shertzer, New J. Phys. **14**, 025003 (2012).

[14] A. A. Kvitsinsky, A. Wu and C.-Y. Hu, J. Phys. B **28**, 275 (1995).

[15] S. L. Yakovlev, C.-Y. Hu and D. Caballero, J. Phys. B **40**, 1675 (2007).

[16] R. Lazauskas, J. Phys. B **50**, 055201 (2017).

[17] M. V. Volkov, E. A. Yarevsky and S. L. Yakovlev, Europhys. Lett. **110**, 30006 (2015).

[18] M. Valdes, M. Dufour, R. Lazauskas and P.-A. Hervieux, Phys. Rev. A **97**, 012709 (2018).

[19] V. A. Gradusov, V. A. Roudnev and S. L. Yakovlev, Atoms **4**, 9 (2016).

[20] S. L. Yakovlev and Z. Papp, Theor. Math. Phys. **163**, 666 (2010).

[21] V. A. Gradusov, V. A. Roudnev, E. A. Yarevsky and S. L. Yakovlev, J. Phys. B **52**, 055202 (2019).

[22] N. W. Schellingerhout, L. P. Kok and G. D. Bosveld, Phys. Rev. A **40**, 5568 (1989).

[23] Y. Saad, *Iterative methods for sparse linear systems*. SIAM, 2003.

[24] B. Bialecki and G. Fairweather, J. Comput. Appl. Math. **46**, 369 (1993).

[25] V. Roudnev and S. Yakovlev, Comput. Phys. Commun. **126**, 162 (2000).

[26] Y. K. Ho and Z.-C. Yan, Phys. Rev. A **70**, 032716 (2004).

[27] K. Varga, J. Mitroy, J. Zs. Mezei and A. T. Kruppa, Phys. Rev. A **77**, 044502 (2008).

[28] R.-M. Yu, Y.-J. Cheng, L.-G. Jiao and Y.-J. Zhou, Chin. Phys. Lett. **29**, 053401 (2012).

[29] M. Umair and S. Jonsell, J. Phys. B **47**, 225001 (2014).

[30] M. Gailitis and R. Damburg, Sov. Phys. JETP **17**, 1107 (1963).

[31] M. Gailitis and R. Damburg, Proc. Phys. Soc. **82**, 192 (1963).

[32] C.-Y. Hu, D. Caballero and Z. Papp, Phys. Rev. Lett. **88**, 063401 (2002).

[33] I. I. Fabrikant, A. W. Bray, A. S. Kadyrov and I. Bray, Phys. Rev. A **94**, 012701 (2016).

[34] B. H. Bransden, C. J. Noble and R. J. Whitehead, J. Phys. B **34**, 2267 (2001).

[35] C. M. Rawlins, A. S. Kadyrov and I. Bray, Phys. Rev. A **97**, 012707 (2018).

[36] Y. Z. Zhang, R. M. Yu, S. X. Li, X. D. Song and L. G. Jiao, J. Phys. B **48**, 175206 (2015).

[37] A. Igarashi and I. Shimamura, Phys. Rev. A **56**, 4733 (1997).

[38] A. Igarashi and I. Shimamura, Phys. Rev. A **70**, 012706 (2004).

[39] M.-M. Liu, H.-L. Han, S.-H. Gu and T.-Y. Shi, Chin. Phys. Lett. **29**, 013101 (2012).

[40] A. I. Baz', Ya. B. Zel'dovich and A. M. Perelomov, *Scattering, reactions and decay in nonrelativistic quantum mechanics*. Israel Program for Scientific Translations, Jerusalem, 1969.

[41] N. Elander and E. Yarevsky, Phys. Rev. A **57**, 3119 (1998).